

pubs.acs.org/NanoLett Letter

Stark Effects of Rydberg Excitons in a Monolayer WSe₂ P-N Junction

Zhen Lian, Yun-Mei Li, Li Yan, Lei Ma, Dongxue Chen, Takashi Taniguchi, Kenji Watanabe, Chuanwei Zhang, and Su-Fei Shi*



Cite This: Nano Lett. 2024, 24, 4843-4848



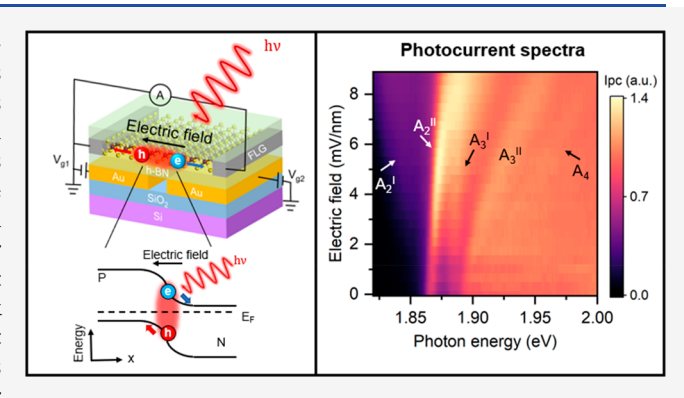
ACCESS I

Metrics & More

Article Recommendations

Supporting Information

ABSTRACT: The enhanced Coulomb interaction in two-dimensional semiconductors leads to tightly bound electron—hole pairs known as excitons. The large binding energy of excitons enables the formation of Rydberg excitons with high principal quantum numbers (n), analogous to Rydberg atoms. Rydberg excitons possess strong interactions among themselves as well as sensitive responses to external stimuli. Here, we probe Rydberg exciton resonances through photocurrent spectroscopy in a monolayer WSe₂ p—n junction formed by a split-gate geometry. We show that an external in-plane electric field not only induces a large Stark shift of Rydberg excitons up to quantum principal number 3 but also mixes different orbitals and brightens otherwise dark states such as 3p and 3d. Our study provides an exciting platform for



engineering Rydberg excitons for new quantum states and quantum sensing.

KEYWORDS: Rydberg excitons, p-n junction, photocurrent spectroscopy, Stark shift, orbital mixing

The reduced screening in 2D enhances the Coulomb interaction and gives rise to tightly bound electron—hole pairs, known as excitons, in monolayer transition-metal dichalcogenides (TMDCs).^{1–5} Excitons in TMDCs exhibit enhanced light—matter interaction and play an important role in the optical and optoelectronic properties of monolayer TMDCs.⁶ Excitons are tunable by external stimuli such as electrostatic doping,^{7,8} electric field,^{9,10} and magnetic field,^{11–13} making them promising in applications ranging from solar energy harvesting to quantum information science.^{6,14–16} Enhancing exciton—exciton interactions and the response of excitons to external stimuli is critical for realizing those applications. For example, the Stark shift allows the manipulation of the exciton energy through an electric field, while the effect is relatively small for the tightly bound intralayer exciton in monolayer TMDCs.

Rydberg exciton is a natural choice as it can be sensitively controlled through an external electric field owing to the large dipole moment. Similar to the energy states in a hydrogen atom, the energy states of an exciton can be described by a series of discrete states known as the excitonic Rydberg series, distinguished by their principal quantum number n and angular quantum number l. Rydberg excitons refer to the excitons with high-order quantum principal numbers (n > 1), analogous to Rydberg atoms. Previous works have demonstrated that the ground state, also known as the 1s exciton, exhibits a quadratic Stark shift and tunable dissociation rate under an in-plane electric field. We expect a much-enhanced Stark shift from Rydberg excitons due to their more extended wave function

and, hence, a much larger induced dipole moment, compared with the 1s exciton.

In this work, we measure the photocurrent spectra^{9,11,19–21} of a monolayer WSe₂ p-n junction formed by a split gate geometry, with the electric field tunable via the combination of the two gate voltages. Previously, we have employed photocurrent spectroscopy under a magnetic field to resolve Rydberg excitons in monolayer WSe2 with record high principal number n up to 11,11 compared with the state-ofart absorption spectroscopy that revealed Rydberg exciton up to n = 5 in monolayer TMDCs. 1,3,12,13 Here, photocurrent spectroscopy enables us to investigate the excitonic response under a tunable electric field beyond the diffraction limit, with the p-n junction defined by a split gate with a spacing of 240 nm. We reveal the excitonic Stark effect of Rydberg excitons with an n up to 3. Remarkably, the electric field results in the mixing of the optically bright s states and the otherwise dark p and d states, resulting in new bright exciton states with hybridized orbitals that are highly tunable by the electric field. The excited states exhibit an energy shift and splitting as large as 96 meV (2s and 2p exciton under the electric field of 15

Received: January 10, 2024 Revised: March 23, 2024 Accepted: March 27, 2024 Published: April 12, 2024





Nano Letters pubs.acs.org/NanoLett Lette

mV/nm), which are orders of magnitude larger than the shift of the ground state (1s) exciton (\sim 2 meV) due to their larger radii. Our results show that the 2D Rydberg excitons are highly tunable by the in-plane electric field.

■ PHOTOCURRENT RESPONSE FROM WSe₂ p−n JUNCTION

We fabricated the monolayer WSe₂ device in a split-gate configuration, as shown in Figure 1a. A typical device is

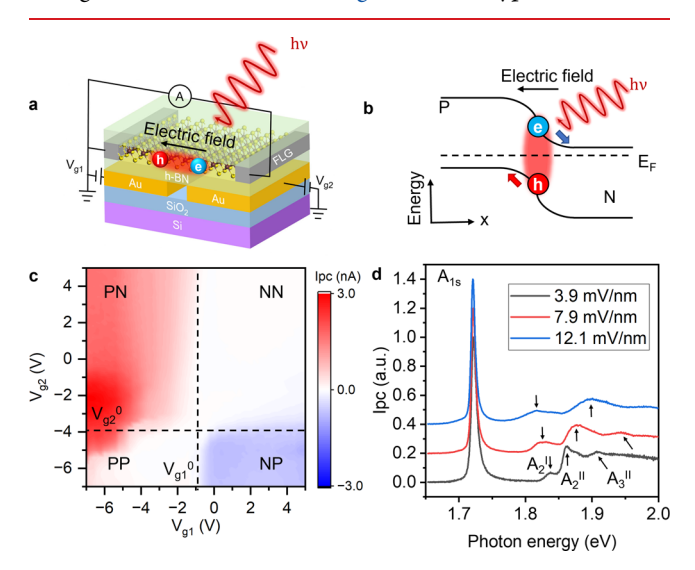


Figure 1. Photocurrent spectra from a monolayer WSe₂ p—n junction. (a) A schematic of the WSe₂ split-gate device. (b) A schematic of the band diagram and the photovoltaic effect of the WSe₂ p—n junction. (c) The photocurrent response from device D1 as a function of both $V_{\rm g1}$ and $V_{\rm g2}$. The photocurrent was measured using pulsed laser excitation centered at 1.96 eV with a power of 100 μ W. (d) Photocurrent spectra measured from device D1 under different electric fields with an offset of 0.2 for better illustration. The magnitude of the photocurrent in (d) is normalized by the magnitude of the 1s exciton. All data shown in Figure 1 were measured at 77 K.

composed of a monolayer WSe2 connected by two few-layer graphene (FLG) as contact electrodes, sandwiched by the top and bottom h-BN layers. The final device is placed on two 3/ 22 nm Ti/Au gate electrodes laterally separated by a gap of ~240 nm, which serve as two back gate electrodes of the device (gate 1 and gate 2). The split gate configuration allows the independent control of the doping levels of the two areas of the monolayer WSe₂ above gate electrodes 1 and 2 (region 1 and region 2) by applying independent gate voltages (V_{g1} and $V_{\rm g2}$) to the two gate electrodes. We then focus a laser beam with the photon energy of 1.96 eV (filtered output from a white laser) on the spot between regions 1 and 2, with the beam spot size about 4 μ m, and collect the photocurrent response. A color plot of the photocurrent response as a function of $V_{\rm g1}$ and $V_{\rm g2}$ measured with 100 $\mu{\rm W}$ laser excitation from a typical device D1 at 77 K is shown in Figure 1c. Clearly, the photocurrent response can be separated into four distinct regions (quadrants), separated by the lines corresponding to $V_{\rm g1}=V_{\rm g1}^0$ and $V_{\rm g2}=V_{\rm g2}^0$ in Figure 1c. In the PN quadrant of Figure 1c ($V_{\rm g1}< V_{\rm g1}^0$ and $V_{\rm g2}> V_{\rm g2}^0$), region 1 is p-doped while region 2 is n-doped. The device exhibits a positive photocurrent response due to the photovoltaic effect arising from the built-in field of the p-n junction (shown schematically in Figure 1b). On the other hand, the NP quadrant $(V_{\rm g1} > V_{\rm g1}^{\rm o}$

and $V_{\rm g2} < V_{\rm g2}^0$) corresponds to the n-p configuration, and the photocurrent switches the sign to be negative since the p-n junction reverses the direction of the built-in electric field. The photocurrent responses from the other two quadrants can be explained by the p-p and n-n configurations: The built-in field is small in these cases and so is the photocurrent magnitude.

We then focus on the PN quadrant in Figure 1c and discuss the electric field dependence of the photocurrent spectra. We applied opposite voltages to gates 1 and 2 $(V_{g2} = -V_{g1} = V_g)$ to apply the in-plane electric field. As we increase the value of V_g , we expect the width of the depletion region of the PN junction to decrease due to the increased doping level in regions 1 and 2, resulting in an enhanced built-in electric field strength. Using an analytical approach, 9,22,23 we calculate the lateral electric field strength F as a function of V_{g} , with details shown in the Supporting Information section 2. In Figure 1d we show the photocurrent spectra measured at three different electric field strengths, 3.9, 7.9, and 12.1 mV/nm. Each peak on the photocurrent spectra represents the absorption resonance of an excitonic state. The most prominent feature in the spectra is a strong absorption peak at 1.721 eV, which corresponds to the 1s state of the WSe₂ A-exciton and is denoted as A_{1s}. It is worth noting that we do not observe any trion peaks, which are typically 20–30 meV below the A-exciton peak, ^{24,25} suggesting the photocurrent response arises selectively from the depletion region of the junction. At energies higher than the resonance of A_{1s} , we observe three weaker excitonic peaks at F = 3.9 mV/nm, which are denoted as A₂, A₂, and A₃ and are located at 1.838, 1.863, and 1.908 eV, respectively. A₂ and A₂ exhibit considerable energy shifts in opposite directions under increasing electric field F. The redshift of A₂ and the blueshift of A_2^{II} are 8 and 14 meV, respectively, at F = 7.9 mV/nm and further increase to 21 and 38 meV, respectively, at F = 12.1mV/nm. The blueshift of A_3^{II} is even larger in magnitude, reaching 70 meV at F = 12.1 mV/nm.

STARK EFFECTS OF EXCITONS

To quantitatively understand the shift of each excitonic peak, we plot the detailed electric-field-dependent photocurrent spectra in Figure 2a–c. Characteristic linecuts from the color plots are also shown in Figure 2d. It is evident that the peak position of A_{1s} (black dots in Figure 2a) is a quadratic function of F, which can be expressed by $E_{1s} = E_{1s}^0 - \alpha F^2$, where E_{1s}^0 is the energy of A_{1s} at zero electric field. From the fitting, we determine $\alpha = 8.0 \pm 0.2 \text{ eV}/(\text{V/nm})^2$, consistent with what has been extracted from the photocurrent spectra of A exciton as a function of electric field $(10 \pm 2 \text{ eV}/(\text{V/nm})^2)$. In the electric field range between 4 and 15 mV/nm, the energy shifts of A_2^{I} and A_2^{II} are approximately linear functions of F, given by $E_n = E_n^0 + \beta F$ (Figure 2b). The fitted values of β are -2.0 ± 0.2 and $4.7 \pm 0.2 \text{ eV} \cdot \text{nm} \cdot \text{V}^{-1}$ for A_2^{I} and A_2^{II} , respectively.

We attribute the shifting and the splitting of the excitonic peaks to the excitonic Stark effects, which are a result of energy shift due to the external electric field modified exciton wave functions. ^{9,10,26–30} To quantitatively evaluate these effects, we calculate the energy of each excitonic state using the nonhydrogenic Keldysh potential ^{31,32} as the effective Coulomb interaction. Following the approach outlined in our previous work, ¹¹ we obtained the energies of the s, p, and d states for Rydberg excitons with $n \leq 3$ (calculation details in methods and Supporting Information section 4), as shown in Table 1. We note that under zero electric field only the s states are the bright states. Our result shows the 1s and 2s states possess a

Nano Letters pubs.acs.org/NanoLett Letter

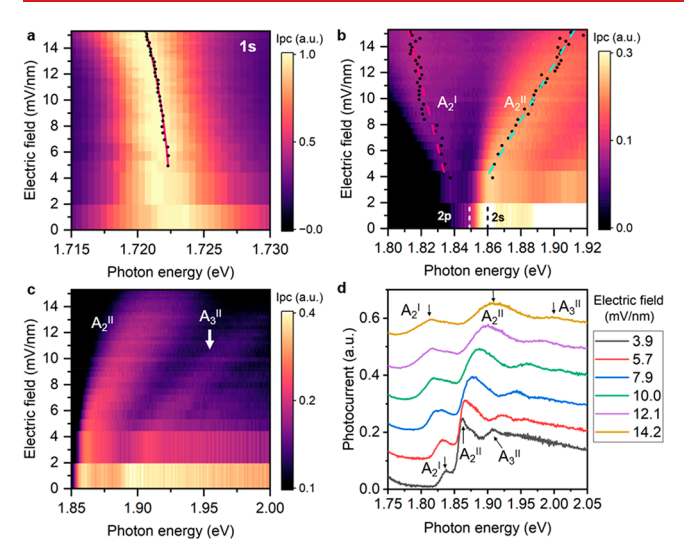


Figure 2. Excitonic Stark effects in the WSe₂ p-n junction. (a-c) Color plots of the photocurrent spectra as a function of the in-plane electric field for Rydberg states corresponding to n=1, 2, and 3, respectively. The black dots denote the extracted peak positions. The red line in (a) is the fitting of the 1s peak position to a quadratic function of electric field F. The red and cyan dashed lines in (b) are the fitting of the $A_2^{\rm I}$ and $A_2^{\rm II}$ peak positions to a linear function of the electric field, respectively. (d) The line cuts of the photocurrent spectra at six different electric field values. The temperature is 77 K for all the measurements shown in Figure 2. The magnitude of the photocurrent in (a-d) is normalized by the magnitude of the 1s exciton.

Table 1. Calculated Binding Energies of Rydberg Excitons with s, p, and d Orbitals at Zero Electric Field

	n = 1	n = 2	n = 3
$Eb_{\rm ns}~({ m meV})$	161.2	37.4	16.1
$Eb_{\rm np}~({ m meV})$		48.3	19.1
Eb_{nd} (meV)			20.5

binding energy of 161.2 and 37.4 meV, respectively. The optically dark 2p state lies slightly below the 2s state and has a binding energy of 48.3 meV. It is worth noting that the 2p and 2s degeneracy is lifted in 2D due to the Keldysh potential, compared with the 2D hydrogen model. It is also worth mentioning that the 2p lies at a lower energy than 2s, a result of the reduced screening for more spread wave function of 2p. The same bandgap, together with the larger binding energy of 2p than 2s, makes the 2p resonance lower in energy, which is a unique feature of 2D excitons. The same argument can be extended to n = 3 states, which we will discuss later.

We then quantitatively investigate the energies of the Rydberg excitons in the presence of an in-plane electric field. The Hamiltonian describing the interaction between a 2D exciton and an in-plane electric field be written as

$$H^e = -eFx \tag{1}$$

where e is the elementary charge, F is the electric field, and x is the coordinate in the direction of the electric field.

As the 1s exciton is well-separated from the states with a higher principal number, its energy in the presence of an external in-plane electric field can be calculated by the secondorder perturbation theory, which yields

$$E_{1s} = E_{1s}^{0} - 2 \sum_{n} \frac{|\langle 1s|H^{e}|np\rangle|^{2}}{E_{np}^{0} - E_{1s}^{0}} = E_{1s} - \alpha F^{2}$$
(2)

where $|np\rangle$ denotes the p-state exciton wave function with principal number n. $E^0_{\rm np}$ and $E^0_{\rm 1s}$ denote the energy of the np state and 1s state at zero electric field, respectively (details in Supporting Information section 5).

Based on Eqn. 1, the value of α is around 9.92 eV/(V/nm)², consistent with the reported values from previous theoretical $(9.8-10.4 \text{ eV/(V/nm)}^2)^{9,29,30}$ and experimental $(10 \pm 2 \text{ eV/(V/nm)}^2)^9$ works, and also agrees well with the value of $8.0 \pm 0.2 \text{ eV/(V/nm)}^2$ extracted from our experiment.

For states with n > 1, their energy separations are comparable to the large Stark energy shift. As a result, the electric field is strong enough to induce a hybridization between multiple excitonic Rydberg states with distinct n and l numbers. Using the exciton wave functions at zero electric field as bases, the interaction term is given by $\langle n'l'|H^e|nl\rangle$. The nature of $A_2^{\rm II}$ can be qualitatively understood with the hybridization between the 2p state and the 2s state, while the details could be revealed more clearly from the photocurrent spectra at a lower temperature, as discussed below.

To resolve the fine features resulting from the Stark splitting corresponding to n = 3, we measured the electric field dependence of the photocurrent spectra at the temperature of 6 K, as shown in Figure 3a,b. At the higher-energy side of A_2^{II} ,

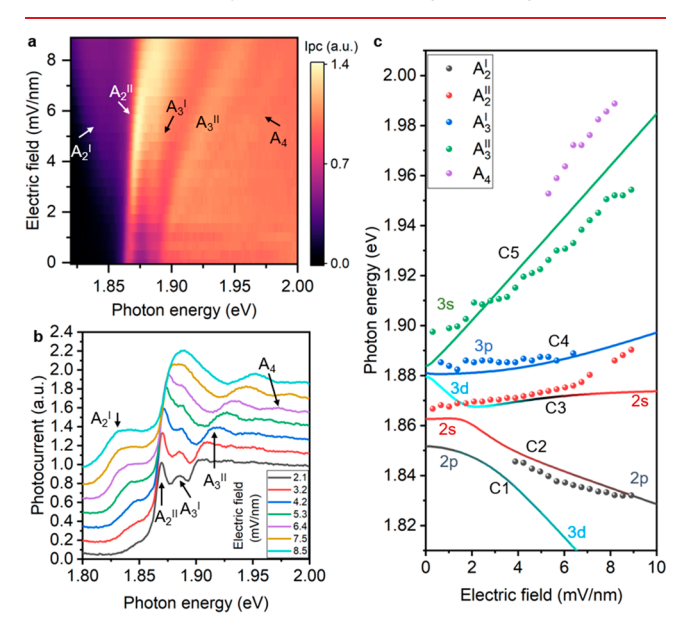


Figure 3. Excitonic Stark effects of Rydberg excitons with n = 3. (a) Color map of the photocurrent spectra as a function of the electric field near the 3s state of monolayer WSe₂ taken at 6 K. (b) The linecuts at seven electric field values from (a). The dots in (c) are the peak positions extracted from (a). The dashed lines are the theoretical exciton energies calculated by considering the hybridization between multiple exciton orbitals.

we observed three high-energy peaks, denoted as A_3^I , A_3^{II} , and A_4 , which shift linearly under an electric field, with their slopes being 0.5 \pm 0.2, 7.7 \pm 0.2, and 12.4 \pm 0.7 eV·nm·V⁻¹, respectively. The low-energy branch A_3^I emerges around 17 meV below A_3^{II} at a relatively low electric field of 2 mV/nm, while the high-energy branch A_4 is resolvable at an electric field above 4 mV/nm.

We now develop a quantitative understanding of the orbital hybridization effect. Using the original $2p_x$, 2s, $3d_{x^2-y^2}$, $3p_x$, and 3s orbitals as the bases, we solve the eigenvalues and eigenfunctions of the interaction Hamiltonian, which lead to the resonance energies of the hybridized excitons as a function of the electrical field shown as the lines in Figure 3c. As the electric field introduces the mixing of different orbital components, the original $2p_{x\nu}$ 2s, $3d_{x^2-y^2}$, $3p_{x\nu}$ and 3s orbitals, labeled as 2p, 2s, 3d, 3p, and 3s at zero electric field (Figure 3c), will mix and generate five dispersive curves as C1-C5 in Figure 3c. At the high electric field limit, we also label the major components of C1, C2, and C3, with the calculated components of different orbital bases shown in Supporting Information section 6. To compare the calculation with our experimental data, we show the peak positions extracted from Figure 3a (solid dots) along with C1-C5 in Figure 3c. It can be found that our theoretical model can explain most features of the photocurrent spectra, including the opposite shift between A_2^{I} and A_2^{II} and the increased separation between A_3^{I} and A₃¹¹ at the increased electric field. Below an electric field of 2 mV/nm, the angular quantum number l is approximately a good quantum number for these excitonic states. As the electric field tunes two states close in energies, the interaction results in the transferring of their main orbital components. Our results show that the field dependence of A₂ is consistent with curve C2. At the electric field as high as 8 mV/nm, the C2 is still visible in the photocurrent spectra due to the finite oscillator strength inherited from the original 2s and 3s orbitals, despite the main component being 2p. A₂^{II} is mainly from the 2s orbital, corresponding to curve C2 for F < 2 mV/nm and C3 for F > 2 mV/nm. Here, we did not observe the level avoiding between C2 and C3, likely due to the experimental uncertainty induced by the finite peak width. We note that theoretically there should be another dispersive branch, curve C1, below A₂^{II}. However, it is not observed in the photocurrent spectra, possibly because of the strong dissociation effect of the 3d orbital, which is the main component of C3 at the high electric field, despite finite oscillator strength transferred from 2s (see details in Supporting Information section 6). Also, the 3d nature might broaden the associated resonance significantly so that the finite oscillator strength distributed over a broad range of energy cannot be resolved from the already broad A₂ peaks, as shown in Figure 3b. The electric field dependence of $A_3^{\rm I}$ and $A_3^{\rm II}$ matches the dispersion of curves C4 and curve C5. The visibility of the A_3^1 is a result of the hybridization of the original 3s, 3p, and even 2s states, which transfer some oscillator strength from 3s and 2s to C4 at a finite electric field and make the original dark 3p state (C4 at zero electric field) bright. The energy of A₄ is obviously higher than the predicted energies of states with n = 3, suggesting that it corresponds to an excitonic state with a higher n number. The A4 peak is significantly broader and weaker in strength than other resonances, and we refrain from a quantitative understanding in this work. It is worth noting that at the field ranging from 6 to 9 mV/nm, Rydberg exciton with principal number n = 4 is likely to be dissociated. The nature of A₄ is intriguing and will be explored

In summary, we employed photocurrent spectra to probe the Rydberg exciton resonances from a monolayer WSe_2 p-n junction. We have observed significant Stark effects on Rydberg excitons with principal numbers up to n=3. The electric field introduces significant mixing of different orbitals

and brightens the otherwise dark states such as 3p and 3d. The electric field, therefore, induces a large energy shift observable in the photocurrent spectra, more than 1 order of magnitude larger than that of 1s exciton. Our works thus pave the way for utilizing Rydberg excitons in the application of quantum sensing.

METHODS

Device Fabrication. The patterns of the split-gate electrodes were defined using the standard electron-beam lithography technique using PMMA as a resist. Three nanometer Ti and 22 nm Au were deposited using electron-beam evaporation. After metal deposition, a lift-off process was performed in acetone and isopropanol. The 2D material flakes were exfoliated onto polydimethylsiloxane (PDMS) films. The bottom h-BN, monolayer WSe₂ (from HQ graphene), few-layer graphene, and top h-BN flakes were transferred on to the electrode layer by layer using a dry-transfer technique³³ reported previously. The optical image of the device can be found in Supporting Information Section 1.

Photocurrent Measurement. To perform photocurrent spectroscopy, the sample was mounted into a cryostat with an optical window and an electrical feedthrough. Broadband white light with a repetition rate of 10 MHz and a pulse width of 100 ps was generated using a supercontinuum laser source (YSL Photonics) and focused into a monochromator (Princeton Instruments). A particular wavelength was selected by using a diffraction grating. The monochromatic light at the exit of the monochromator was collimated using a lens and then focused into a spot with a diameter of around 4 μ m on the sample using an objective ($50 \times$, NA = 0.55). A mechanical chopper was used to apply the AC modulation to the incident laser. The gate voltages on the sample were applied using Keithley 2400 multimeters. The photocurrent from the sample was collected using a preamplifier (Stanford Research Systems), a lock-in amplifier (Stanford Research Systems), and a data acquisition card (National Instruments).

Electric Field Calculation. The in-plane electric field as a function of gate voltages at 77 K was calculated using an analytical method developed by previous works. 9,22,23 The monolayer WSe₂ was first treated as a metal plate to obtain a charge density distribution. The electric field is then calculated by solving the Laplace equation in the 2D channel using the boundary conditions defined by the charge distribution. The details of this calculation can be found in Supporting Information section 2. Due to the increased contact resistance at 6 K, the electric field in Figure 3 was calibrated by interpolating the $A_2^{\rm I} - A_2^{\rm II}$ splitting obtained from Figure 2 (See Supporting Information Section 3 for details).

Calculation of Exciton Energies. The energy of each excitonic Rydberg state at zero electric field was calculated using the same method described by our previous work. We numerically solved the two-body Schrodinger equation in two dimensions using the nonhydrogenic Keldysh potential 31,32 as the effective Coulomb interaction. The eigenstates and eigenenergy were obtained numerically by expanding the wave function in terms of Bessel bases. The bandgap of WSe₂ ($E_{\rm g}$) was set to be 1.90 eV. The surrounding dielectric constant ε and the 2D polarizability $\chi_{\rm 2D}$ in the Keldysh potential are $4.5\varepsilon_0$ and 0.718 nm, respectively. The reduced mass of exciton $m_{\rm r}$ is $0.2m_0$, where m_0 is the electron mass. The energy of the 1s state under an in-plane electric field was calculated using the second-order perturbation theory. The energies of the Rydberg

Nano Letters pubs.acs.org/NanoLett Letter

states with n=2 and 3 were calculated by considering the electric field-induced hybridization of s, p, and d orbitals, using the $2p_x$, 2s, $3d_{x^2-y^2}$, $3p_x$ and 3s orbitals as the bases. The calculation details can be found in Supporting Information sections 4 and 5.

ASSOCIATED CONTENT

Supporting Information

The Supporting Information is available free of charge at https://pubs.acs.org/doi/10.1021/acs.nanolett.4c00134.

Optical image of the device, details about electric field calculation, exciton energies with and without the inplane electric field, calculated orbital components and energies of hybridized excitons, and Stark shift of 1s exciton at 6 K (PDF)

AUTHOR INFORMATION

Corresponding Author

Su-Fei Shi — Department of Physics, Carnegie Mellon University, Pittsburgh 15213 Pennsylvania, United States; Department of Chemical and Biological Engineering, Rensselaer Polytechnic Institute, Troy 12180 New York, United States; orcid.org/0000-0001-5158-805X; Email: sufeis@andrew.cmu.edu

Authors

Zhen Lian — Department of Physics, Carnegie Mellon University, Pittsburgh 15213 Pennsylvania, United States; Department of Chemical and Biological Engineering, Rensselaer Polytechnic Institute, Troy 12180 New York, United States

Yun-Mei Li — Department of Physics, School of Physical Science and Technology, Xiamen University, Xiamen 361005, China; orcid.org/0000-0002-8074-467X

Li Yan – Department of Chemical and Biological Engineering, Rensselaer Polytechnic Institute, Troy 12180 New York, United States

Lei Ma – Department of Chemical and Biological Engineering, Rensselaer Polytechnic Institute, Troy 12180 New York, United States

Dongxue Chen – Department of Chemical and Biological Engineering, Rensselaer Polytechnic Institute, Troy 12180 New York, United States

Takashi Taniguchi — International Center for Materials Nanoarchitectonics, National Institute for Materials Science, Tsukuba 305-0044, Japan; orcid.org/0000-0002-1467-3105

Kenji Watanabe — Research Center for Functional Materials, National Institute for Materials Science, Tsukuba 305-0044, Japan; © orcid.org/0000-0003-3701-8119

Chuanwei Zhang — Department of Physics, University of Texas at Dallas, Richardson 75080 Texas, United States; Department of Physics, Washington University in St Louis, St. Louis 63105 Missouri, United States

Complete contact information is available at: https://pubs.acs.org/10.1021/acs.nanolett.4c00134

Author Contributions

^O(Z.L., Y.-M.L., L.Y.) These authors contributed equally to this work.

Author Contributions

S.-F. S. conceived the project. Z. L. fabricated devices and performed measurements. Y.-M. L. and C. Z. performed the calculations. T. T. and K. W. grew the BN crystals. S.-F. S, Z. L, L. Y., and L. M. analyzed the data. S.-F. S. supervised the project. S.-F. S. and Z. L. wrote the manuscript with input from all authors.

Notes

The authors declare no competing financial interest.

ACKNOWLEDGMENTS

We thank Prof. Yong-Tao Cui for the helpful discussions. This work is mainly supported by NSF Grant ECCS-2139692. S.-F. S. also acknowledges support from NSF grants DMR-1945420, DMR-2104902, and NYSTAR through Focus Center-NY-RPI Contract C180117. The device fabrication was supported by the Micro and Nanofabrication Clean Room (MNCR) at Rensselaer Polytechnic Institute (RPI). Y.-M. L. acknowledges support from Grant No. 2022YFA1204700 from the Ministry of Science and Technology of the People's Republic of China. K. W. and T. T. acknowledge support from JSPS KAKENHI (Grant Nos. 19H05790, 20H00354, and 21H05233). The optical spectroscopy measurements were supported by the AFOSR DURIP awards through Grants FA9550-20-1-0179 and FA9550-23-1-0084. C. Z. acknowledges support from NSF (PHY-2409943, OMR-2228725, ECCS-2411394) and AFOSR (FA9550-20-1-0220).

REFERENCES

- (1) He, K.; Kumar, N.; Zhao, L.; Wang, Z.; Mak, K. F.; Zhao, H.; Shan, J. Tightly Bound Excitons in Monolayer WSe₂. *Phys. Rev. Lett.* **2014**, *113*, 26803.
- (2) Zhu, B.; Chen, X.; Cui, X. Exciton Binding Energy of Monolayer WS₂. Sci. Rep **2015**, 5, 9218.
- (3) Chernikov, A.; Berkelbach, T. C.; Hill, H. M.; Rigosi, A.; Li, Y.; Aslan, O. B.; Reichman, D. R.; Hybertsen, M. S.; Heinz, T. F. Exciton Binding Energy and Nonhydrogenic Rydberg Series in Monolayer WS₂. *Phys. Rev. Lett.* **2014**, *113*, No. 076802.
- (4) Wang, G.; Chernikov, A.; Glazov, M. M.; Heinz, T. F.; Marie, X.; Amand, T.; Urbaszek, B. Colloquium: Excitons in Atomically Thin Transition Metal Dichalcogenides. *Rev. Mod. Phys.* **2018**, *90*, 21001.
- (5) Xiao, J.; Zhao, M.; Wang, Y.; Zhang, X. Excitons in Atomically Thin 2D Semiconductors and Their Applications. *Nanophotonics* **2017**, *6*, 1309.
- (6) Mak, K. F.; Shan, J. Photonics and Optoelectronics of 2D Semiconductor Transition Metal Dichalcogenides. *Nat. Photonics* **2016**, *10*, 216.
- (7) Mak, K. F.; He, K.; Lee, C.; Lee, G. H.; Hone, J.; Heinz, T. F.; Shan, J. Tightly Bound Trions in Monolayer MoS₂. *Nat. Mater.* **2013**, 12, 207.
- (8) Ross, J. S.; Wu, S.; Yu, H.; Ghimire, N. J.; Jones, A. M.; Aivazian, G.; Yan, J.; Mandrus, D. G.; Xiao, D.; Yao, W.; Xu, X. Electrical Control of Neutral and Charged Excitons in a Monolayer Semiconductor. *Nat. Commun.* **2013**, *4*, 1474.
- (9) Massicotte, M.; Vialla, F.; Schmidt, P.; Lundeberg, M. B.; Latini, S.; Haastrup, S.; Danovich, M.; Davydovskaya, D.; Watanabe, K.; Taniguchi, T.; Fal'ko, V. I.; Thygesen, K. S.; Pedersen, T. G.; Koppens, F. H. L. Dissociation of Two-Dimensional Excitons in Monolayer WSe₂. *Nat. Commun.* **2018**, *9*, 1633.
- (10) Zhu, B.; Xiao, K.; Yang, S.; Watanabe, K.; Taniguchi, T.; Cui, X. In-Plane Electric-Field-Induced Orbital Hybridization of Excitonic States in Monolayer WSe₂. *Phys. Rev. Lett.* **2023**, *131*, 36901.
- (11) Wang, T.; Li, Z.; Li, Y.; Lu, Z.; Miao, S.; Lian, Z.; Meng, Y.; Blei, M.; Taniguchi, T.; Watanabe, K.; Tongay, S.; Smirnov, D.; Zhang, C.; Shi, S.-F. Giant Valley-Polarized Rydberg Excitons in

Nano Letters pubs.acs.org/NanoLett Letter

- Monolayer WSe₂ Revealed by Magneto-Photocurrent Spectroscopy. *Nano Lett.* **2020**, *20*, 7635.
- (12) Stier, A. V.; Wilson, N. P.; Velizhanin, K. A.; Kono, J.; Xu, X.; Crooker, S. A. Magnetooptics of Exciton Rydberg States in a Monolayer Semiconductor. *Phys. Rev. Lett.* **2018**, *120*, 57405.
- (13) Goryca, M.; Li, J.; Stier, A. V.; Taniguchi, T.; Watanabe, K.; Courtade, E.; Shree, S.; Robert, C.; Urbaszek, B.; Marie, X.; Crooker, S. A. Revealing Exciton Masses and Dielectric Properties of Monolayer Semiconductors with High Magnetic Fields. *Nat. Commun.* **2019**, *10*, 4172.
- (14) Liu, X.; Hersam, M. C. 2D Materials for Quantum Information Science. *Nat. Rev. Mater.* **2019**, *4*, 669.
- (15) Yu, H.; Liu, G.-B.; Tang, J.; Xu, X.; Yao, W. Moiré Excitons: From Programmable Quantum Emitter Arrays to Spin-Orbit—Coupled Artificial Lattices. *Sci. Adv.* **2017**, *3*, e1701696.
- (16) Li, Y.-M.; Li, J.; Shi, L.-K.; Zhang, D.; Yang, W.; Chang, K. Light-Induced Exciton Spin Hall Effect in van Der Waals Heterostructures. *Phys. Rev. Lett.* **2015**, *115*, 166804.
- (17) Ye, Z.; Cao, T.; O'Brien, K.; Zhu, H.; Yin, X.; Wang, Y.; Louie, S. G.; Zhang, X. Probing Excitonic Dark States in Single-Layer Tungsten Disulphide. *Nature* **2014**, *513*, 214.
- (18) Wu, F.; Qu, F.; MacDonald, A. H. Exciton Band Structure of Monolayer MoS₂. Phys. Rev. B **2015**, 91, 75310.
- (19) Klots, A. R.; Newaz, A. K. M.; Wang, B.; Prasai, D.; Krzyzanowska, H.; Lin, J.; Caudel, D.; Ghimire, N. J.; Yan, J.; Ivanov, B. L.; Velizhanin, K. A.; Burger, A.; Mandrus, D. G.; Tolk, N. H.; Pantelides, S. T.; Bolotin, K. I. Probing Excitonic States in Suspended Two-Dimensional Semiconductors by Photocurrent Spectroscopy. Sci. Rep 2014, 4, 6608.
- (20) Massicotte, M.; Schmidt, P.; Vialla, F.; Schädler, K. G.; Reserbat-Plantey, A.; Watanabe, K.; Taniguchi, T.; Tielrooij, K. J.; Koppens, F. H. L. Picosecond Photoresponse in van Der Waals Heterostructures. *Nat. Nanotechnol* **2016**, *11*, 42.
- (21) Lian, Z.; Jiang, Z.; Wang, T.; Blei, M.; Qin, Y.; Washington, M.; Lu, T.-M.; Tongay, S.; Zhang, S.; Shi, S.-F. Anisotropic Band Structure of TiS₃ Nanoribbon Revealed by Polarized Photocurrent Spectroscopy. *Appl. Phys. Lett.* **2020**, *117*, 073101.
- (22) Glazman, L. I.; Larkin, I. A. Lateral Position Control of an Electron Channel in a Split-Gate Device. *Semicond. Sci. Technol.* **1991**, *6*, 32.
- (23) Chklovskii, D. B.; Shklovskii, B. I.; Glazman, L. I. Electrostatics of Edge Channels. *Phys. Rev. B* **1992**, *46*, 4026.
- (24) Courtade, E.; Semina, M.; Manca, M.; Glazov, M. M.; Robert, C.; Cadiz, F.; Wang, G.; Taniguchi, T.; Watanabe, K.; Pierre, M.; Escoffier, W.; Ivchenko, E. L.; Renucci, P.; Marie, X.; Amand, T.; Urbaszek, B. Charged Excitons in Monolayer WSe₂: Experiment and Theory. *Phys. Rev. B* **2017**, *96*, 85302.
- (25) Jones, A. M.; Yu, H.; Schaibley, J. R.; Yan, J.; Mandrus, D. G.; Taniguchi, T.; Watanabe, K.; Dery, H.; Yao, W.; Xu, X. Excitonic Luminescence Upconversion in a Two-Dimensional Semiconductor. *Nat. Phys.* **2016**, *12*, 323.
- (26) Lederman, F. L.; Dow, J. D. Theory of Electroabsorption by Anisotropic and Layered Semiconductors. I. Two-Dimensional Excitons in a Uniform Electric Field. *Phys. Rev. B* **1976**, *13*, 1633.
- (27) Scharf, B.; Frank, T.; Gmitra, M.; Fabian, J.; Žutić, I.; Perebeinos, V. Excitonic Stark Effect in MoS₂ Monolayers. *Phys. Rev. B* **2016**, *94*, 245434.
- (28) Haastrup, S.; Latini, S.; Bolotin, K.; Thygesen, K. S. Stark Shift and Electric-Field-Induced Dissociation of Excitons in Monolayer MoS₂ and HBN/MoS₂ Heterostructures. *Phys. Rev. B* **2016**, 94, 41401.
- (29) Cavalcante, L. S. R.; da Costa, D. R.; Farias, G. A.; Reichman, D. R.; Chaves, A. Stark Shift of Excitons and Trions in Two-Dimensional Materials. *Phys. Rev. B* **2018**, *98*, 245309.
- (30) Pedersen, T. G. Exciton Stark Shift and Electroabsorption in Monolayer Transition-Metal Dichalcogenides. *Phys. Rev. B* **2016**, *94*, 125424.
- (31) Keldysh, L. V. Coulomb Interaction in Thin Semiconductor and Semimetal Films. J. Exp. Theor. Phys. Lett. 1979, 29, 716.

- (32) Berkelbach, T. C.; Hybertsen, M. S.; Reichman, D. R. Theory of Neutral and Charged Excitons in Monolayer Transition Metal Dichalcogenides. *Phys. Rev. B* **2013**, *88*, 45318.
- (33) Castellanos-Gomez, A.; Buscema, M.; Molenaar, R.; Singh, V.; Janssen, L.; van der Zant, H. S. J.; Steele, G. A. Deterministic Transfer of Two-Dimensional Materials by All-Dry Viscoelastic Stamping. *2d Mater.* **2014**, *1*, 011002.